

Orbital hyperfine interaction and qubit dephasing in carbon nanotube quantum dots

Gábor Csiszár¹ and András Pályi^{1,2,3}

¹*Institute of Physics, Eötvös University, Budapest, Hungary*

²*MTA-BME Condensed Matter Research Group, Budapest University of Technology and Economics, Budapest, Hungary*

³*Kavli Institute for Theoretical Physics China, Beijing, P. R. China*

(Dated: September 10, 2014)

Hyperfine interaction (HF) is of key importance for the functionality of solid-state quantum information processing, as it affects qubit coherence and enables nuclear-spin quantum memories. In this work, we complete the theory of the basic hyperfine interaction mechanisms (Fermi contact, dipolar, orbital) in carbon nanotube quantum dots by providing a theoretical description of the orbital HF. We find that orbital HF induces an interaction between the nuclear spins of the nanotube lattice and the valley degree of freedom of the electrons confined in the quantum dot. We show that the resulting nuclear-spin-electron-valley interaction (i) is approximately of Ising type, (ii) is essentially local, in the sense that a radius- and dot-length-independent atomic interaction strength can be defined, and (iii) has an atomic interaction strength that is comparable to the combined strength of Fermi contact and dipolar interactions. We argue that orbital HF provides a new decoherence mechanism for single-electron valley qubits and spin-valley qubits in a range of multi-valley materials. We explicitly evaluate the corresponding inhomogeneous dephasing time T_2^* for a nanotube-based valley qubit.

PACS numbers: 73.63.Kv, 73.63.Fg, 71.70.Ej, 76.20.+q

I. INTRODUCTION

Carbon nanotubes (CNT) provide a promising platform^{1,2} for quantum information processing.³⁻⁶ In non-metallic CNTs, one or a few electrons can be captured in an electrically defined quantum dot (QD), potentially allowing for coherent control of the electrons' internal (spin and valley) degrees of freedom.

Hyperfine interaction (HF) between the nuclear spins of the lattice and the electrons in the QD can be either a nuisance or an asset in this context. On the one hand, a randomized nuclear-spin ensemble induces decoherence of a spin-based electronic qubit.⁷⁻⁹ On the other hand, HF is the mechanism that allows for information transfer between the electronic state and the nuclear spins, a critical step for utilizing nuclear spins as long-lived quantum memories.¹⁰⁻¹⁴ Remarkably, the abundance of nuclear spins in the CNT lattice can be increased (decreased) by isotopic enrichment¹⁵⁻¹⁷ (purification) of the spin-half ^{13}C nuclei, which have a natural abundance of $\sim 1\%$. The fundamental importance of HF in these nanostructures is also highlighted by the possibility of HF-mediated nuclear magnetism in one-dimensional solids¹⁸⁻²⁰ including ^{13}C -enriched CNTs.

Partly motivated by these attractive features, a series of experiments were carried out with clean CNTs, aiming to control and measure the spin and valley degrees of freedom of electrons confined in QDs.^{16,17,21,22} Surprisingly, two of these experiments using ^{13}C -enriched samples revealed effects compatible with an atomic HF strength that is two orders of magnitude larger than theoretically calculated^{9,23} and measured via nuclear magnetic resonance.^{24,25} The resolution of this discrepancy is an open problem,² bearing strong relevance for HF-related phenomena in CNTs.

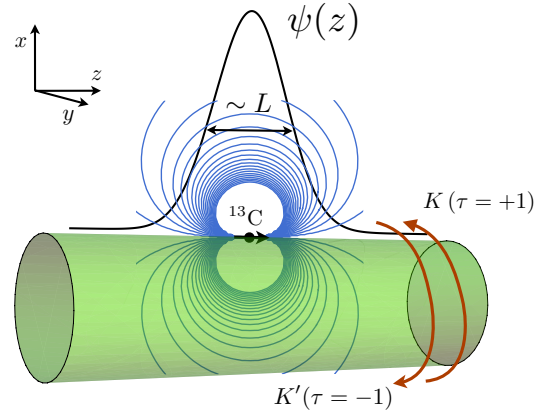


FIG. 1. Carbon nanotube quantum dot with a single spin-carrying ^{13}C nucleus. Arrows labeled with K ($\tau = +1$) and K' ($\tau = -1$) represent the two electronic valley states, moving to opposite directions around the nanotube circumference. The black solid line and $\psi(z)$ represents the longitudinal envelope-function characterizing the ground-state of an electron confined in the QD. Blue lines represent the dipole magnetic field created by the spin of the ^{13}C nucleus.

The interesting prospects in quantum information processing and nuclear magnetism, as well as the theory-experiment mismatch of the coupling strength, stimulated efforts²⁵⁻³⁰ toward a more complete understanding of HF in carbon-based nanostructures. These works explore the consequences of two out of the three basic mechanisms of HF,³¹ Fermi contact (a.k.a. isotropic) and dipolar, and exclude the third one, orbital HF (OHF).³² It should be noted that the consequences of OHF in nuclear magnetic resonance of CNTs^{33,34} and graphene³⁵ have been analyzed.

In this work, we complete the theoretical description of hyperfine effects in CNT QDs by elucidating the role of the OHF. We show that this mechanism provides an effective interaction between a nuclear spin and the valley degree of freedom of the electron: the simple argument (see Fig. 1) is that the binary valley quantum number K, K' labels electronic states circulating along the CNT circumference in the clockwise and counter-clockwise direction,^{36,37} respectively, and therefore the electron has a valley-dependent orbital magnetic moment that feels the dipole magnetic field created by the nuclear spin. Using the envelope-function model (Dirac equation) for the electrons, and focusing on the case when the longitudinal electronic wave length λ exceeds the nanotube radius R , we show that the resulting nuclear-spin-electron-valley interaction (i) is approximately of Ising type, (ii) is essentially local, in the sense that a radius- and dot-length-independent atomic interaction strength can be defined, and (iii) has an atomic interaction strength that is comparable to the combined strength of Fermi contact and dipolar interactions. We argue that the inhomogeneous dephasing time T_2^* of single-electron valley qubits and spin-valley qubits is affected by the OHF, and explicitly evaluate T_2^* for a valley qubit.

II. ORBITAL HYPERFINE INTERACTION WITH THE ELECTRONIC VALLEY DEGREE OF FREEDOM

Here, we provide an analytical description of the OHF-mediated coupling between the nuclear spin of a single ^{13}C atom residing in a CNT QD and the valley degree of freedom of a single electron confined to the same QD. To this end, the electron will be described by the canonical envelope-function model² of CNTs (Dirac equation). In the terminology introduced by Yafet,³² our approach describes the ‘long-range’ part of OHF; the ‘short-range’ part of OHF is shown to be absent in CNTs in the tight-binding framework of Ref. 9. Our description remains qualitatively valid for any type of spin-carrying nucleus.

The setup and the reference frame is shown in Fig. 1. The spin-carrying ^{13}C nucleus is located at $\mathbf{r}_0 = (R, 0, z_0)$. The nuclear spin has a dipole moment $g_N \mu_N$, and therefore it creates a vector potential

$$\mathbf{A}(\mathbf{r}) = \frac{\mu_0}{4\pi} g_N \mu_N \frac{\mathbf{I} \times (\mathbf{r} - \mathbf{r}_0)}{|\mathbf{r} - \mathbf{r}_0|^3} \equiv \mathbf{I} \times \mathbf{v}(\mathbf{r} - \mathbf{r}_0). \quad (1)$$

Here, $g_N \approx 1.41$ is the g-factor of the ^{13}C nucleus,⁹ and $\mu_N \approx 5.05 \times 10^{-27}$ J/T is the nuclear magneton. The nuclear spin vector operator \mathbf{I} is represented by one half times the vector of Pauli matrices.

Technically, OHF between the nuclear spin and the electron arises because the vector potential \mathbf{A} created by the nuclear spin enters the kinetic term of the envelope-function Hamiltonian via $\mathbf{p} \mapsto \mathbf{p} + e\mathbf{A}$. The kinetic term, describing an electron in the conduction or valence band,

reads²

$$H_0 + H_{\text{OHF}} = v_F \{ \tau_3 \sigma_1 [p_c + e A_c(\mathbf{r})] + \sigma_2 [p_t + e A_t(\mathbf{r})] \}, \quad (2)$$

where $c(t)$ is the circumferential (longitudinal) coordinate on the surface of the CNT, $\sigma_{1,2}$ are sublattice Pauli matrices, and H_{OHF} is defined as the parts of the rhs that contain the vector potential. Note that our choice of the reference frame (Fig. 1) allows us to use t and z interchangeably. In Eq. (2), we introduced the circumferential and longitudinal projections of the vector potential, $A_c(\mathbf{r}) = \hat{\mathbf{c}}(c) \cdot \mathbf{A}(\mathbf{r})$ and $A_t(\mathbf{r}) = \hat{\mathbf{t}} \cdot \mathbf{A}(\mathbf{r})$, respectively, where $\hat{\mathbf{c}}(c) = (-\sin \frac{c}{R}, \cos \frac{c}{R}, 0)$, $\hat{\mathbf{t}} = (0, 0, 1)$, and $\mathbf{r} \equiv \mathbf{r}(c, t) = (R \cos \frac{c}{R}, R \sin \frac{c}{R}, t)$. While p_c is the circumferential momentum quantum number set by the periodic boundary condition along the CNT circumference, p_t is the longitudinal momentum operator. The form (2) of the Hamiltonian is valid for any chirality; here we focus on CNTs with a finite gap (i.e., $p_c \neq 0$) allowing for electrostatic QD confinement.

Using Eqs. (1) and (2), the OHF Hamiltonian can be written as

$$H_{\text{OHF}} = e v_F \tau_3 \sigma_1 \varepsilon_{\alpha\beta\gamma} I_\alpha v_\beta (\mathbf{r} - \mathbf{r}_0) \hat{c}_\gamma, \quad (3)$$

where $\varepsilon_{\alpha\beta\gamma}$ is the Levi-Civita symbol, the Einstein summation convention is used, and the valley-independent term have been omitted as it is irrelevant for valley dynamics.

For simplicity, we assume $p_c > 0$, and anticipate that a sign change in p_c implies a sign change of the coupling constants C_α (defined below). Then, an electronic low-energy energy eigenstate in valley $\tau \in (K, K') \equiv (+1, -1)$ of the conduction band of the electrostatically defined QD is approximately described by the four-component spinor envelope function

$$\Psi_\tau(c, t) = |\tau\rangle \otimes |\chi\rangle \otimes \frac{e^{i\tau(p_c/\hbar)c}}{\sqrt{2\pi R}} \psi(t), \quad (4)$$

where $|\tau = +1\rangle = (1, 0)^T$ or $|\tau = -1\rangle = (0, 1)^T$ represent the valley state, $|\chi\rangle = (1, 1)^T/\sqrt{2}$ characterizes the sublattice amplitudes at the bottom of the conduction band, and $\psi(t)$ is the longitudinal envelope function of the electron. The normalization condition $\int_{-\infty}^{\infty} dt \int_0^{2\pi R} dc \Psi^\dagger(c, t) \Psi(c, t) = 1$ demands $\int_{-\infty}^{\infty} dt |\psi(t)|^2 = 1$. Note that by writing the envelope function $\Psi_\tau(c, t)$ as a product of a circumferential and longitudinal component in Eq. (4), we implicitly assumed that the confinement potential is longitudinal (i.e., independent of c).

The effective Hamiltonian describing the nuclear-spin-electron-valley interaction is obtained via first-order degenerate perturbation theory, i.e., by projecting H_{OHF} to the two-dimensional subspace spanned by Ψ_K and $\Psi_{K'}$:

$$H_{\text{OHF}}^{(\text{eff})} \equiv P H_{\text{OHF}} P = \frac{1}{2} \tau_3 \sum_{\alpha=x,y,z} C_\alpha I_\alpha, \quad (5)$$

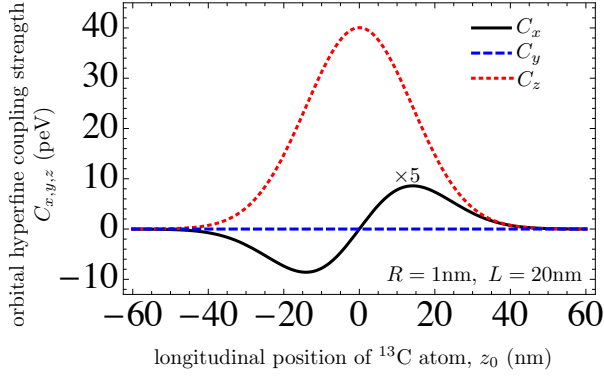


FIG. 2. Orbital hyperfine coupling strengths as functions of the nuclear-spin position in a carbon nanotube quantum dot. The plot is based on Eq. (7) and corresponds to the case of a Gaussian longitudinal envelope function [Eq. (8)]. Note that C_x was multiplied by 5. Axes x, y, z are defined in Fig. 1.

where Eqs. (3), (4), and $P \equiv |\Psi_K\rangle\langle\Psi_K| + |\Psi_{K'}\rangle\langle\Psi_{K'}|$ were used, τ_3 has been redefined as $\tau_3 \equiv |\Psi_K\rangle\langle\Psi_K| - |\Psi_{K'}\rangle\langle\Psi_{K'}|$, and

$$C_\alpha(z_0) = \frac{ev_F}{\pi R} \int_{-\infty}^{\infty} dt |\psi(t)|^2 \int_0^{2\pi R} dc \epsilon_{\alpha\beta\gamma} v_\beta(\mathbf{r} - \mathbf{r}_0) \hat{c}_\gamma. \quad (6)$$

Note that the last integral ($\int dc \dots$) is proportional to the magnetic flux that is piercing the circular cross section of the CNT at height t in the presence of a (classical) nuclear spin that is aligned with axis α .

Now we evaluate the coupling strengths in Eq. (6), in the case where the length scale λ of the spatial variation of the longitudinal envelope function $\psi(z)$ exceeds the radius R of the CNT. This is the relevant case for those experiments that are done with few electrons confined in a ~ 100 nm long QD in a CNT with radius $R \sim 1$ nm. For this case, we will show that

$$C_x(z_0) \approx -2ev_F \frac{\mu_0 g_N \mu_N}{4\pi} [\psi^*(z_0)\psi'(z_0) + c.c.] \quad (7a)$$

$$C_y(z_0) = 0, \quad (7b)$$

$$C_z(z_0) \approx 2ev_F \frac{\mu_0 g_N \mu_N}{4\pi} \frac{1}{R} |\psi(z_0)|^2, \quad (7c)$$

where ψ' is the derivative of ψ with respect to the longitudinal coordinate. Equation (5) together with Eq. (7) form the central result of this work. The dependence of the three coupling strengths $C_{x,y,z}$ on the longitudinal position z_0 of the nuclear spin is shown in Fig. 2, for the case of a CNT with radius $R = 1$ nm and a Gaussian longitudinal envelope function

$$\psi(t) = \frac{1}{\pi^{1/4} \sqrt{L}} e^{-\frac{t^2}{2L^2}} \quad (8)$$

with $L = 20$ nm.

An interpretation of Eq. (7) is as follows. If the nuclear spin is aligned with the CNT axis, then it induces an energy splitting C_z between the two valley states (i.e., a *valley splitting*) of the electron. If the nuclear spin is aligned

radially, then it induces a valley splitting C_x , which is typically much smaller than in the former case, because $(\partial_z \psi)(z_0) \sim \psi(z_0)/\lambda$ is much smaller than $\psi(z_0)/R$ due to the assumed length-scale mismatch $R \ll \lambda$. Finally, if the nuclear spin is aligned orthoradially (i.e., perpendicular to the axial and radial directions) then it does not induce valley splitting. Alternatively, Eqs. (5) and (7) can be interpreted in terms of an effective magnetic field that acts on the nuclear spin and determined by the valley state of the electron. This effective magnetic field has an axial as well as a much smaller radial component, and it has no orthoradial component.

The three coupling strengths $C_{x,y,z}$ expressed in Eq. (7) have qualitatively different dependencies on the longitudinal envelope function ψ . A simple understanding of these differences is gained using the relation between the coupling strengths C_α and the magnetic fluxes piercing the CNT cross sections, discussed after Eq. (6). Figure 3 displays characteristic magnetic field lines piercing circular cross sections of the CNT that are positioned symmetrically with respect to the nuclear spin position, for three different alignments of the nuclear spin. For a radially aligned nuclear spin (Fig. 3a), the fluxes piercing the two cross sections of the tube (orange) are identical in magnitude but differ in sign. Therefore, a homogeneous longitudinal envelope function $\psi(t)$ would imply a zero coupling strength C_x , since the flux contributions of the two cross sections would cancel each other in the $\int dt$ integral of Eq. (6). The inhomogeneity of $\psi(t)$, i.e., the finiteness of ψ' , prevents this cancellation, and allows for a finite coupling strength C_x ; this is reflected by the dependence $C_x \propto \psi'$ of Eq. (7a). For an axially aligned nuclear spin (Fig. 3c), the fluxes piercing the two circular cross sections (orange) of the CNT are identical in sign (and also in magnitude), hence the cancellation affecting C_x is not relevant for C_z . Finally, for an orthoradially aligned nuclear spin (Fig. 3b), the magnetic flux piercing each of the two circular cross sections (orange) of the tube is zero, explaining Eq. (7b).

The results (5) and (7) have the following implications.

(i) In the considered range $\lambda \gg R$, the OHF-induced nuclear-spin-electron-valley interaction is essentially of Ising type, $\propto \tau_3 I_z$. The correction of the form $\propto \tau_3 I_x$ is small since $C_x \ll C_z$. Note that the coupling strength C_x might gain importance in the case $\lambda \sim R$, e.g., in ultrashort CNT QDs,^{38–40} or in QDs where the electron occupies a highly excited, short-wavelength longitudinal mode.

(ii) Even though OHF is long-range in principle, our leading-order result (7c) suggests that it is essentially local under our assumptions, since the strength of the resulting nuclear-spin-electron-valley interaction is determined by the value of the electronic envelope function at the position of the nucleus. In other words, the result (7c) affirms that for practical purposes, the envelope-function Hamiltonian H_{OHF} can be replaced by

$$\tilde{H}_{\text{OHF}} = ev_F \mu_0 g_N \mu_N \delta(c - c_0) \delta(t - t_0) \frac{\tau_3}{2} I_z, \quad (9)$$

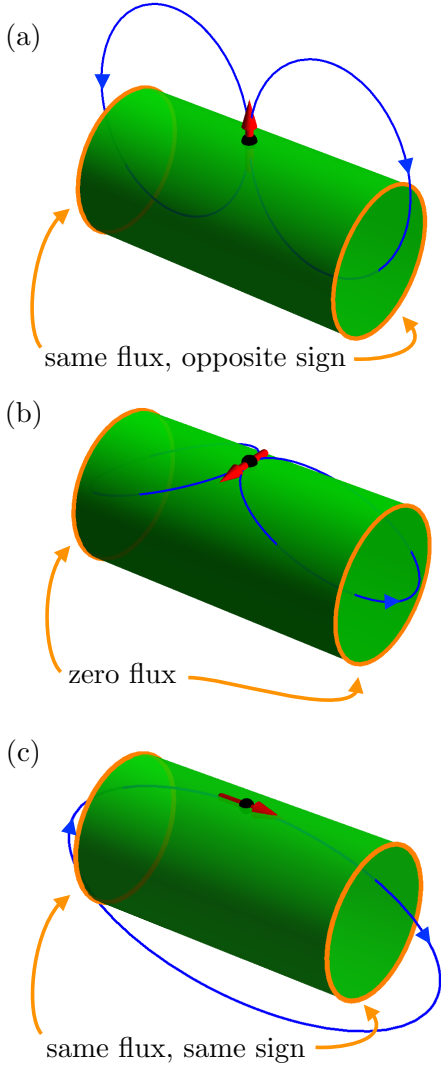


FIG. 3. Nuclear-spin-induced magnetic field lines and magnetic fluxes. Black dot (red arrow) represents the position (alignment) of the nuclear spin. Blue lines are magnetic field lines, and the blue arrowheads indicate their directionality. Orange circles represent two symmetrically positioned circular cross sections of the tube. (a) For a radially aligned nuclear spin, the fluxes piercing the two cross sections (orange) are identical in magnitude but differ in sign. (b) For an orthoradially aligned nuclear spin, the flux piercing both cross sections (orange) are zero. (c) For an axially aligned nuclear spin, the fluxes piercing the cross sections (orange) are identical in magnitude and sign.

since $PH_{\text{OHF}}P = P\tilde{H}_{\text{OHF}}P$. Therefore, an *atomic coupling strength* A of the OHF can be defined via

$$\tilde{H}_{\text{OHF}} = \frac{\Omega_{\text{cell}}}{2} A \delta(c - c_0) \delta(t - t_0) \frac{\tau_3}{2} I_z \quad (10)$$

in analogy with, e.g., the atomic coupling strength of Fermi contact HF in GaAs, see Eq. (2) of Ref. 8. Here $\Omega_{\text{cell}} \approx 5.24 \text{ \AA}^2$ is the area of the graphene unit cell. The atomic coupling strength A can be deduced from Eqs.

(9) and (10):

$$A \approx \frac{2ev_F\mu_0g_N\mu_N}{\Omega_{\text{cell}}} \approx 0.34\mu\text{eV}, \quad (11)$$

where $v_F = 10^6 \text{ m/s}$ was assumed.²

(iii) The estimated atomic coupling strength (11) of the OHF-induced nuclear-spin–electron-valley interaction is comparable to the atomic coupling strength of the combined Fermi contact and dipolar spin HF.^{9,23} This result has the following consequences. (1) In order to provide an accurate assessment of any property or functionality of a CNT-based electronic spin-valley qubit,^{21,22,41–43} the Fermi contact, dipolar and orbital contributions should be treated on an equal footing. (2) Nuclear spins in a CNT QD will induce inhomogeneous dephasing of an electronic valley qubit on a time scale similar to the inhomogeneous dephasing time of a spin qubit or spin-valley qubit. We present a detailed analysis of the latter point in Sec. III.

For completeness we also provide the OHF Hamiltonian describing the nuclear-electron spin-valley interaction in the presence of more than one nuclear spins \mathbf{I}_k . Here, $k \in 1 \dots N$ where N is the number of atoms interacting with the electron in the QD, and \mathbf{I}_k is the spin-half nuclear spin operator if site k has a ^{13}C atom and zero otherwise. The k th atom is assumed to be located at the position specified by the circumferential c_k and longitudinal t_k coordinates, corresponding to the real-space position $\mathbf{r}_k \equiv (x_k, y_k, z_k) = (R \cos(c_k/R), R \sin(c_k/R), t_k)$. The effective OHF Hamiltonian then reads

$$H_{\text{OHF}}^{(\text{eff})} = \frac{1}{2} \tau \sum_{k=1}^N M_k \mathbf{I}_k, \quad (12)$$

where M_k is the 3×3 local orbital hyperfine tensor

$$M_k = \begin{pmatrix} 0 & 0 & 0 \\ 0 & 0 & 0 \\ C_x(t_k) \cos(c_k/R) & C_x(t_k) \sin(c_k/R) & C_z(t_k) \end{pmatrix} \quad (13)$$

and C_x and C_z are given in Eq. (7).

This Section is concluded by proving Eq. (7). First, we prove Eq. (7a) by evaluating C_x using Eq. (6), the definition of \mathbf{v} via Eq. (1), and the definition of $\hat{\mathbf{c}}$ given below Eq. (2). After introducing the dimensionless quantities $\varphi = c/R$ and $\zeta = \frac{t-z_0}{R}$, we find

$$C_x(z_0) = -\frac{ev_F}{\pi R} \frac{\mu_0 g_N \mu_N}{4\pi} \int_{-\infty}^{\infty} d\zeta |\psi(z_0 + R\zeta)|^2 \times \int_0^{2\pi} d\varphi \frac{\zeta \cos(\varphi)}{(2 - 2\cos(\varphi) + \zeta^2)^{3/2}} \quad (14)$$

Note that although the integrand is singular at the position of the nuclear spin, i.e., for $(c, t) = (0, z_0)$, that is, for $(\varphi, \zeta) = (0, 0)$, the integral does converge, similarly to the case of OHF in graphene.³⁵ Importantly, the integrand in the second line of Eq. (14) decays for $\zeta \gg 1$ as $\sim 1/\zeta^2$, suggesting that the integral is dominated by the range $|\zeta| \lesssim 1$, that is, by the spatial

range $|z - z_0| \lesssim R$. Since this spatial range is narrow in comparison with the length scale λ characterizing the spatial variation of the longitudinal envelope function ψ , we can estimate the value of the integral by expanding the term $|\psi|^2$ term up to first order in ζ : $|\psi(z_0 + R\zeta)|^2 \approx |\psi(z_0)|^2 + R\zeta[\psi^*(z_0)\psi'(z_0) + c.c.]$. The integral containing the zeroth-order term vanishes as its integrand is an odd function of ζ . The integral containing the first-order term is finite though, providing the estimate Eq. (7a) above. Technically, the $C_y = 0$ result in Eq. (7b) follows from the fact that the $\alpha = y$ integrand in Eq. (6) is an antisymmetric function of $c \in [0, 2\pi R]$ with respect to $c = \pi R$. Finally, the derivation of Eq. (7c) is similar to that of Eq. (7a). The difference here is that the integral will be dominated by the zeroth-order term in the ζ expansion of $|\psi(z_0 + R\zeta)|^2$, hence higher-order terms can be neglected.

III. INHOMOGENEOUS DEPHASING OF A VALLEY QUBIT

HF leads to information loss via decoherence for spin qubits in conventional semiconductors^{8,44} as well as in carbon nanostructures.^{9,29,30} One form of decoherence is inhomogeneous dephasing, which arises due to a nuclear-spin-induced random component in the qubit's Larmor frequency, and is characterized by the time scale T_2^* , usually called the inhomogeneous dephasing time. To our knowledge, the T_2^* of valley qubits^{45–49} due to HF has not yet been investigated. Based on the result of the previous Section, here we evaluate T_2^* for a valley qubit formed in the conduction-band ground state of a CNT QD, as a function of the CNT radius R , the QD length L , and the abundance $\nu \in [0, 1]$ of ^{13}C atoms.

We assume that the valley states of the single electron forming the valley qubit are energy-split ($\hbar\omega_L$) by a longitudinal magnetic field and/or spin-orbit interaction, and the qubit is tuned far away from the K - K' anticrossing^{50,51} caused by valley mixing. The valley qubit is prepared in a superposition state $\Psi(t = 0) = \frac{1}{\sqrt{2}}(|\Psi_K\rangle + |\Psi_{K'}\rangle)$. It interacts with the nuclear spin bath that is completely disordered to a good approximation. The Hamiltonian reads

$$H = \frac{1}{2}\hbar\omega_L\tau_3 + H_{\text{OHF}}^{(\text{eff})}, \quad (15)$$

where $H_{\text{OHF}}^{(\text{eff})}$ is given in Eq. (12), and we neglect C_x .

Following Merkulov et al.,⁸ we disregard the slow dynamics of the nuclear spin bath, and describe the nuclear spins as being frozen during the time evolution of the electronic valley state. The influence of the nuclear spin ensemble is expressed via the HF-induced random correction $\delta\omega = \frac{1}{\hbar}\sum_{k,\alpha} M_{k;3,\alpha} I_{k,\alpha} \approx \frac{1}{\hbar}\sum_k C_z(z_k) I_{k,z}$ of the valley Larmor frequency ω_L . In the presence of many nuclear spins, the correction $\delta\omega$ can be regarded as a Gaussian random variable with the following mean

and variance:

$$\langle\delta\omega\rangle \equiv \frac{1}{\hbar}\langle\sum_k C_z(z_k) I_{k,z}\rangle = 0, \quad (16)$$

$$\sigma^2 \equiv \langle(\delta\omega)^2\rangle = \frac{\nu}{4\hbar}\sum_k C_z^2(z_k). \quad (17)$$

Here the average $\langle.\rangle$ refers to both ensemble averaging for the nuclear spin states as well as disorder averaging for the possible spatial configurations of the spin-carrying nuclei. Correspondingly, we used $\langle I_{k,\alpha}\rangle = 0$ and $\langle I_{k,\alpha} I_{k',\alpha'}\rangle = \frac{\nu}{4}\delta_{kk'}\delta_{\alpha\alpha'}$, and ν is the abundance of spin-carrying nuclei.

The polarization vector of the valley qubit in the initial state $\Psi(0)$ is $\mathbf{p} \equiv \langle\Psi(0)|\boldsymbol{\tau}|\Psi(0)\rangle = (1, 0, 0)^T$. A straightforward calculation⁸ shows that the time evolution of the valley polarization $\mathbf{p}(t)$, averaged for the random nuclear-spin configurations, reads

$$\langle\mathbf{p}\rangle(t) \equiv \langle\Psi(t)|\boldsymbol{\tau}|\Psi(t)\rangle = \begin{pmatrix} \cos(\omega_L t) \\ \sin(\omega_L t) \\ 0 \end{pmatrix} e^{-(t/T_2^*)^2}, \quad (18)$$

where

$$T_2^* = \sqrt{2}/\sigma = \frac{1}{\sqrt{\nu}} \frac{2\sqrt{2}\hbar}{\sqrt{\sum_k C_z^2(z_k)}}. \quad (19)$$

For a box-type longitudinal envelope function, i.e., if $\psi(z) = 1/\sqrt{L}$ within a QD of length L , we find

$$T_2^* \approx \frac{1}{\sqrt{\nu}} 2^{3/2} \sqrt{\pi} \frac{\sqrt{\Omega_{\text{cell}}}\hbar}{e\nu_F\mu_0 g_N \mu_N} \sqrt{LR}, \quad (20)$$

where Eqs. (7c) and (19) were used. For a natural (non-isotope-enriched) CNT QD containing $N = 6 \times 10^5$ atoms, we estimate $T_2^* \approx 266 \mu\text{s}$, comparable to the theoretically estimated spin dephasing time.⁹ This is not surprising, regarding that the orbital HF atomic coupling strength estimated in the previous Section was also comparable to the spin HF (combined Fermi contact and dipolar) atomic coupling strength.

For the Gaussian longitudinal envelope function defined in Eq. (8), which provides a more realistic description of the ground-state orbital of a QD with parabolic electrostatic confinement, we find the same parameter dependence as for the box-model wave function, with slightly different prefactors:

$$T_2^* \approx \frac{1}{\sqrt{\nu}} 2^{7/4} \pi^{3/4} \frac{\sqrt{\Omega_{\text{cell}}}\hbar}{e\nu_F\mu_0 g_N \mu_N} \sqrt{LR}. \quad (21)$$

Note that if the relatively small coupling strength C_x corresponding to a radially aligned nuclear spin is taken into account, then the inhomogeneous dephasing time is $(1 - \frac{R^2}{2L^2})$ times the rhs of Eq. (21), i.e., the correction due to C_x is second order in the small quantity R/L . The coupling strength C_x might gain importance and significantly contribute to the T_2^* in ultrashort CNT QDs,^{38–40}

where $L \sim R$, or for electrons that occupy a highly excited longitudinal mode of a QD.

The interpretation of the results (20) and (21) is straightforward. An increasing ^{13}C abundance ν leads to shorter T_2^* , and the inverse-square-root dependence on ν originates from the completely randomized character of the nuclear spin bath. The inverse linear dependence of T_2^* on the parameters setting the interaction strength (e , v_F , μ_0 , g_N , μ_N) and the square-root dependence on the geometrical parameters R and L are natural consequences of the parametric dependencies of the orbital HF coupling strengths in Eq. (7).

IV. DISCUSSION

(1) A natural consequence of our results is that the nuclear-spin–electron-valley interaction arising from OHF contributes to the dephasing of spin-valley qubits in carbon nanotubes.^{22,41} To our knowledge, this contribution has not been analyzed to date. As the strength of this interaction is comparable to the nuclear-spin–electron-spin^{9,23} and nuclear-spin–electron-valley²⁶ interactions arising from the Fermi contact and dipolar mechanisms, it is expected that the hyperfine-limited inhomogeneous dephasing time of a spin-valley qubit has a scale similar to that of the spin qubit (see Ref. 9) and the valley qubit (see Sec. III). A detailed calculation of T_2^* of the spin-valley qubit, which could quantify, e.g., the dependence of T_2^* on the direction of the homogeneous magnetic field, is yet to be done.

(2) We emphasize that valley-qubit coherence might be affected by mechanisms other than OHF. For example, spin-independent potential disorder, similarly to the case of silicon-based heterostructure QDs,^{52–54} makes the valley qubit susceptible to electric fields,⁴⁶ including electrical fluctuations caused by phonons or nearby electrodes. In addition, if a CNT valley qubit is tuned by an axial magnetic field to the K - K' anticrossing (e.g., to 0.11 T in Fig. 2e of Ref. 51), then valley mixing due to Fermi contact and dipolar HF²⁶ can also induce qubit dephasing. Exploring the competition and interplay of various valley-qubit decoherence mechanisms is an interesting future direction.

(3) Importantly, our present effort, which completes the theoretical description of the basic hyperfine mechanisms for CNT QDs, does not explain the comparatively strong hyperfine coupling strength deduced from the ex-

periments of Refs. 16 and 17.

(4) HF between electronic spin qubits and nuclear spins can be harmful, as described above, from the quantum information perspective. It can also be an asset though: in principle, nuclear spins can be used as long-lived quantum memories,^{11–14} and information transfer between the electronic and nuclear degrees of freedom can be mediated by HF. Furthermore, enrichment (purification) of the ^{13}C abundance is a feasible way^{15–17} to enhance (suppress) hyperfine effects.

(5) In certain inversion-symmetry-broken two-dimensional multi-valley materials, such as monolayer transition-metal dichalcogenides⁵⁵ or gapped graphene,⁵⁶ the electronic states acquire a finite valley-dependent magnetic moment. This magnetic moment is inherently coupled with the nuclear spins of the crystal lattice via OHF; therefore, if an electron is confined in a QD in these materials,^{57,58} then its operation as a valley qubit or as a spin-valley qubit will be influenced by the OHF-induced nuclear-spin–electron-valley interaction in a similar fashion as in a CNT. The OHF and its consequences in such two-dimensional materials are yet to be explored.

In conclusion, we have shown that orbital hyperfine interaction couples the nuclear spins residing in a carbon nanotube quantum dot and the valley degree of freedom of the electron confined in the quantum dot. We provided a quantitative analysis of this interaction, and found that it is essentially a local Ising-type interaction, which is as strong as the nuclear-spin–electron-spin hyperfine interactions (Fermi contact and dipolar). As an application, we evaluated the hyperfine-limited inhomogeneous dephasing time of a single-electron valley qubit, which was found to be in the $\sim 100\mu\text{s}$ range, similar to theoretical estimates for CNT-based spin qubits, but much longer than the measured T_2^* of single-electron spin-valley qubits.

ACKNOWLEDGMENTS

We thank P. Boross, B. Dóra, P. Nagy, M. Rudner, F. Simon, Á. Szabados and G. Tichy for useful discussions. We acknowledge funding from the EU Marie Curie Career Integration Grant CIG-293834 (CarbonQubits), the OTKA Grant PD 100373, and the EU ERC Starting Grant CooPairEnt 258789. A. P. is supported by the János Bolyai Scholarship of the Hungarian Academy of Sciences.

¹ F. Kuemmeth, H. Churchill, P. Herring, and C. Marcus, *Materials Today* **13**, 18 (2010).

² E. Laird, F. Kuemmeth, G. Steele, K. Grove-Rasmussen, J. Nygard, K. Flensberg, and L. P. Kouwenhoven, arXiv:1403:6113 (unpublished).

³ D. Loss and D. P. DiVincenzo, *Phys. Rev. A* **57**, 120

(1998).

⁴ R. Hanson, L. P. Kouwenhoven, J. R. Petta, S. Tarucha, and L. M. K. Vandersypen, *Rev. Mod. Phys.* **79**, 1217 (2007).

⁵ R. Hanson and D. D. Awschalom, *Nature* **453**, 1043 (2008).

- ⁶ D. D. Awschalom, L. C. Bassett, A. S. Dzurak, E. L. Hu, and J. R. Petta, *Science* **339**, 1174 (2013).
- ⁷ F. H. L. Koppens, C. Buizert, K. J. Tielrooij, I. T. Vink, K. C. Nowack, T. Meunier, L. P. Kouwenhoven, and L. M. K. Vandersypen, *Nature* **442**, 766 (2006).
- ⁸ I. A. Merkulov, A. L. Efros, and M. Rosen, *Phys. Rev. B* **65**, 205309 (2002).
- ⁹ J. Fischer, W. A. Coish, D. V. Bulaev, and D. Loss, *Phys. Rev. B* **78**, 155329 (2008).
- ¹⁰ B. E. Kane, *Nature* **393**, 133 (1998).
- ¹¹ J. M. Taylor, C. M. Marcus, and M. D. Lukin, *Phys. Rev. Lett.* **90**, 206803 (2003).
- ¹² M. V. G. Dutt, L. Childress, L. Jiang, E. Togan, J. Maze, F. Jelezko, A. S. Zibrov, P. R. Hemmer, and M. D. Lukin, *Science* **316**, 1312 (2007).
- ¹³ G. D. Fuchs, G. Burkard, P. V. Klimov, and D. D. Awschalom, *Nature Physics* **7**, 789 (2011).
- ¹⁴ J. J. Pla, K. Y. Tan, J. P. Dehollain, W. H. Lim, J. J. L. Morton, F. A. Zwanenburg, D. N. Jamieson, A. S. Dzurak, and A. Morello, *Nature* **496**, 334 (2013).
- ¹⁵ F. Simon, C. Kramberger, R. Pfeiffer, H. Kuzmany, V. Zólyomi, J. Kürti, P. M. Singer, and H. Alloul, *Phys. Rev. Lett.* **95**, 017401 (2005).
- ¹⁶ H. O. H. Churchill, F. Kuemmeth, J. Harlow, A. J. Bestwick, E. I. Rashba, K. Flensberg, C. H. Stwertka, T. Taychatanapat, S. K. Watson, and C. M. Marcus, *Phys. Rev. Lett.* **102**, 166802 (2009).
- ¹⁷ H. O. H. Churchill, A. J. Bestwick, J. W. Harlow, F. Kuemmeth, D. Marcos, C. H. Stwertka, S. K. Watson, and C. M. Marcus, *Nature Physics* **5**, 321 (2009).
- ¹⁸ B. Braunecker, P. Simon, and D. Loss, *Phys. Rev. Lett.* **102**, 116403 (2009).
- ¹⁹ B. Braunecker, P. Simon, and D. Loss, *Phys. Rev. B* **80**, 165119 (2009).
- ²⁰ C. P. Scheller, T.-M. Liu, G. Barak, A. Yacoby, L. N. Pfeiffer, K. W. West, and D. M. Zumbühl, *Phys. Rev. Lett.* **112**, 066801 (2014).
- ²¹ F. Pei, E. A. Laird, G. A. Steele, and L. P. Kouwenhoven, *Nat. Nanotech.* **7**, 630 (2012).
- ²² E. A. Laird, F. Pei, and L. P. Kouwenhoven, *Nat. Nanotech.* **8**, 565 (2013).
- ²³ O. V. Yazyev, *Nano Lett.* **8**, 1011 (2008).
- ²⁴ C. H. Pennington and V. A. Stenger, *Rev. Mod. Phys.* **68**, 855 (1996).
- ²⁵ A. Kiss, A. Pályi, Y. Ihara, P. Wzietek, H. Alloul, P. Simon, V. Zólyomi, J. Koltai, J. Kürti, B. Dóra, et al., *Phys. Rev. Lett.* **107**, 187204 (2011).
- ²⁶ A. Pályi and G. Burkard, *Phys. Rev. B* **80**, 201404 (2009).
- ²⁷ A. A. Reynoso and K. Flensberg, *Phys. Rev. B* **84**, 205449 (2011).
- ²⁸ A. A. Reynoso and K. Flensberg, *Phys. Rev. B* **85**, 195441 (2012).
- ²⁹ M. Fuchs, V. Rychkov, and B. Trauzettel, *Phys. Rev. B* **86**, 085301 (2012).
- ³⁰ M. Fuchs, J. Schliemann, and B. Trauzettel, *Phys. Rev. B* **88**, 245441 (2013).
- ³¹ A. Abragam, *The principles of nuclear magnetism* (Oxford University Press, 1961).
- ³² Y. Yafet, *J. Phys. Chem. Solids* **21**, 99 (1961).
- ³³ S. Latil, L. Henrard, C. Goze Bac, P. Bernier, and A. Rubio, *Phys. Rev. Lett.* **86**, 3160 (2001).
- ³⁴ C. Goze-Bac, S. Latil, P. Lauginie, V. Jourdain, J. Conard, L. Duclaux, A. Rubio, and P. Berniera, *Carbon* **40**, 1825 (2002).
- ³⁵ B. Dóra and F. Simon, *Phys. Rev. Lett.* **102**, 197602 (2009).
- ³⁶ H. Ajiki and T. Ando, *Journal of the Physical Society of Japan* **62**, 1255 (1993).
- ³⁷ E. D. Minot, Y. Yaish, V. Sazonova, and P. L. McEuen, *Nature* **428**, 536 (2004).
- ³⁸ X. Sun, S. Zaric, D. Daranciang, K. Welscher, Y. Lu, X. Li, and H. Dai, *Journal of the American Chemical Society* **130**, 6551 (2008).
- ³⁹ J. O. Island, V. Tayari, S. Yigen, A. C. McRae, and A. R. Champagne, *Applied Physics Letters* **99**, 243106 (2011).
- ⁴⁰ P. Petit, C. Feuillet-Palma, M. L. Della Rocca, and P. Lafarge, *Phys. Rev. B* **89**, 115432 (2014).
- ⁴¹ K. Flensberg and C. M. Marcus, *Phys. Rev. B* **81**, 195418 (2010).
- ⁴² G. Széchenyi and A. Pályi, *Phys. Rev. B* **89**, 115409 (2014).
- ⁴³ E. N. Osika, A. Mrenca, and B. Szafran, arXiv:1403.6970v1 (unpublished).
- ⁴⁴ W. A. Coish and J. Baugh, *physica status solidi (b)* **246**, 2203 (2009), ISSN 1521-3951.
- ⁴⁵ P. Recher, B. Trauzettel, A. Rycerz, Y. M. Blanter, C. W. J. Beenakker, and A. F. Morpurgo, *Phys. Rev. B* **76**, 235404 (2007).
- ⁴⁶ A. Pályi and G. Burkard, *Phys. Rev. Lett.* **106**, 086801 (2011).
- ⁴⁷ G. Y. Wu, N.-Y. Lue, and L. Chang, *Phys. Rev. B* **84**, 195463 (2011).
- ⁴⁸ D. Culcer, A. L. Saraiva, B. Koiller, X. Hu, and S. D. Sarma, *Phys. Rev. Lett.* **108**, 126804 (2012).
- ⁴⁹ N. Rohling and G. Burkard, *New Journal of Physics* **14**, 083008 (2012).
- ⁵⁰ D. V. Bulaev, B. Trauzettel, and D. Loss, *Phys. Rev. B* **77**, 235301 (2008).
- ⁵¹ F. Kuemmeth, S. Ilani, D. C. Ralph, and P. L. McEuen, *Nature* **452**, 448 (2008).
- ⁵² M. Friesen and S. N. Coppersmith, *Phys. Rev. B* **81**, 115324 (2010).
- ⁵³ D. Culcer, X. Hu, and S. Das Sarma, *Phys. Rev. B* **82**, 205315 (2010).
- ⁵⁴ J. K. Gamble, M. A. Eriksson, S. N. Coppersmith, and M. Friesen, *Phys. Rev. B* **88**, 035310 (2013).
- ⁵⁵ D. Xiao, G.-B. Liu, W. Feng, X. Xu, and W. Yao, *Phys. Rev. Lett.* **108**, 196802 (2012).
- ⁵⁶ D. Xiao, W. Yao, and Q. Niu, *Phys. Rev. Lett.* **99**, 236809 (2007).
- ⁵⁷ A. Kormányos, V. Zólyomi, N. D. Drummond, and G. Burkard, *Phys. Rev. X* **4**, 011034 (2014).
- ⁵⁸ P. Recher, J. Nilsson, G. Burkard, and B. Trauzettel, *Phys. Rev. B* **79**, 085407 (2009).